DESY 98–210
December 1998

ISSN 0418–9833

Measurement of Internal Jet Structure in Dijet Production in Deep-Inelastic Scattering at HERA

H1 Collaboration

hep-ex/9901010 9 Jan 1999

Abstract

Internal jet structure in dijet production in deep-inelastic scattering is measured with the H1 detector at HERA. Jets with transverse energies $E_{T,\mathrm{Breit}} > 5\,\mathrm{GeV}$ are selected in the Breit frame employing $k_\perp$ and cone jet algorithms. In the kinematic region of squared momentum transfers $10 < Q^2 \lesssim 120\,\mathrm{GeV}^2$ and x-Bjorken values $2 \cdot 10^{-4} \lesssim x_{\mathrm{Bj}} \lesssim 8 \cdot 10^{-3}$, jet shapes and subjet multiplicities are measured as a function of a resolution parameter. Distributions of both observables are corrected for detector effects and presented as functions of the transverse jet energy and jet pseudo-rapidity. Dependences of the jet shape and the average number of subjets on the transverse energy and the pseudo-rapidity of the jet are observed. With increasing transverse jet energies and decreasing pseudo-rapidities, i.e. towards the photon hemisphere, the jets are more collimated. QCD models give a fair description of the data.

submitted to Nuclear Physics B

H1 Collaboration

C. Adloff[34], V. Andreev[25], B. Andrieu[28], V. Arkadov[35], A. Astvatsatourov[35], I. Ayyaz[29], A. Babaev[24], J. Bähr[35], P. Baranov[25], E. Barrelet[29], W. Bartel[11], U. Bassler[29], P. Bate[22], A. Beglarian[11,40], O. Behnke[11], H.-J. Behrend[11], C. Beier[15], A. Belousov[25], Ch. Berger[1], G. Bernardi[29], T. Berndt[15], G. Bertrand-Coremans[4], P. Biddulph[22], J.C. Bizot[27], V. Boudry[28], W. Braunschweig[1], V. Brisson[27], D.P. Brown[22], W. Brückner[13], P. Bruel[28], D. Bruncko[17], J. Bürger[11], F.W. Büsser[12], A. Buniatian[32], S. Burke[18], G. Buschhorn[26], D. Calvet[23], A.J. Campbell[11], T. Carli[26], E. Chabert[23], M. Charlet[4], D. Clarke[5], B. Clerbaux[4], S. Cocks[19], J.G. Contreras[8,43], C. Cormack[19], J.A. Coughlan[5], M.-C. Cousinou[23], B.E. Cox[22], G. Cozzika[10], J. Cvach[30], J.B. Dainton[19], W.D. Dau[16], K. Daum[39], M. David[10], M. Davidsson[21], A. De Roeck[11], E.A. De Wolf[4], B. Delcourt[27], R. Demirchyan[11,40], C. Diaconu[23], M. Dirkmann[8], P. Dixon[20], W. Dlugosz[7], K.T. Donovan[20], J.D. Dowell[3], A. Droutskoi[24], J. Ebert[34], G. Eckerlin[11], D. Eckstein[35], V. Efremenko[24], S. Egli[37], R. Eichler[36], F. Eisele[14], E. Eisenhandler[20], E. Elsen[11], M. Enzenberger[26], M. Erdmann[14,42,f], A.B. Fahr[12], L. Favart[4], A. Fedotov[24], R. Felst[11], J. Feltesse[10], J. Ferencei[17], F. Ferrarotto[32], M. Fleischer[8], G. Flügge[2], A. Fomenko[25], J. Formánek[31], J.M. Foster[22], G. Franke[11], E. Gabathuler[19], K. Gabathuler[33], F. Gaede[26], J. Garvey[3], J. Gassner[33], J. Gayler[11], R. Gerhards[11], S. Ghazaryan[11,40], A. Glazov[35], L. Goerlich[6], N. Gogitidze[25], M. Goldberg[29], I. Gorelov[24], C. Grab[36], H. Grässler[2], T. Greenshaw[19], R.K. Griffiths[20], G. Grindhammer[26], T. Hadig[1], D. Haidt[11], L. Hajduk[6], M. Hampel[1], V. Haustein[34], W.J. Haynes[5], B. Heinemann[11], G. Heinzelmann[12], R.C.W. Henderson[18], S. Hengstmann[37], H. Henschel[35], R. Heremans[4], I. Herynek[30], K. Hewitt[3], K.H. Hiller[35], C.D. Hilton[22], J. Hladký[30], D. Hoffmann[11], T. Holtom[19], R. Horisberger[33], S. Hurling[11], M. Ibbotson[22], Ç. İşsever[8], M. Jacquet[27], M. Jaffre[27], D.M. Jansen[13], L. Jönsson[21], D.P. Johnson[4], H. Jung[21], H.K. Kästli[36], M. Kander[11], D. Kant[20], M. Kapichine[9], M. Karlsson[21], O. Karschnik[12], J. Katzy[11], O. Kaufmann[14], M. Kausch[11], N. Keller[14], I.R. Kenyon[3], S. Kermiche[23], C. Keuker[1], C. Kiesling[26], M. Klein[35], C. Kleinwort[11], G. Knies[11], J.H. Köhne[26], H. Kolanoski[38], S.D. Kolya[22], V. Korbel[11], P. Kostka[35], S.K. Kotelnikov[25], T. Krämerkämper[8], M.W. Krasny[29], H. Krehbiel[11], D. Krücker[26], K. Krüger[11], A. Küpper[34], H. Küster[2], M. Kuhlen[26], T. Kurča[35], W. Lachnit[11], R. Lahmann[11], D. Lamb[3], M.P.J. Landon[20], W. Lange[35], U. Langenegger[36], A. Lebedev[25], F. Lehner[11], V. Lemaitre[11], R. Lemrani[10], V. Lendermann[8], S. Levonian[11], M. Lindstroem[21], G. Lobo[27], E. Lobodzinska[6,41], V. Lubimov[24], S. Lüders[36], D. Lüke[8,11], L. Lytkin[13], N. Magnussen[34], H. Mahlke-Krüger[11], N. Malden[22], E. Malinovski[25], I. Malinovski[25], R. Maraček[26], P. Marage[4], J. Marks[14], R. Marshall[22], H.-U. Martyn[1], J. Martyniak[6], S.J. Maxfield[19], S.J. McMahon[19], T.R. McMahon[19], A. Mehta[5], K. Meier[15], P. Merkel[11], F. Metlica[13], A. Meyer[11], A. Meyer[11], H. Meyer[34], J. Meyer[11], P.-O. Meyer[2], S. Mikocki[6], D. Milstead[11], R. Mohr[26], S. Mohrdieck[12], M. Mondragon[8], F. Moreau[28], A. Morozov[9], J.V. Morris[5], D. Müller[37], K. Müller[11], P. Murín[17], V. Nagovizin[24], B. Naroska[12], J. Naumann[8], Th. Naumann[35], I. Négri[23], P.R. Newman[3], H.K. Nguyen[29], T.C. Nicholls[11], F. Niebergall[12], C. Niebuhr[11], Ch. Niedzballa[1], H. Niggli[36], O. Nix[15], G. Nowak[6], T. Nunnemann[13], H. Oberlack[26], J.E. Olsson[11], D. Ozerov[24], P. Palmen[2], V. Panassik[9], C. Pascaud[27], S. Passaggio[36], G.D. Patel[19], H. Pawletta[2], E. Perez[10], J.P. Phillips[19], A. Pieuchot[11], D. Pitzl[36], R. Pöschl[8], G. Pope[7], B. Povh[13], K. Rabbertz[1], J. Rauschenberger[12], P. Reimer[30], B. Reisert[26], D. Reyna[11], H. Rick[11], S. Riess[12], E. Rizvi[3], P. Robmann[37], R. Roosen[4], K. Rosenbauer[1], A. Rostovtsev[24,12], F. Rouse[7], C. Royon[10], S. Rusakov[25], K. Rybicki[6], D.P.C. Sankey[5], P. Schacht[26], J. Scheins[1], F.-P. Schilling[14], S. Schleif[15], P. Schleper[14],

D. Schmidt[34], D. Schmidt[11], L. Schoeffel[10], V. Schröder[11], H.-C. Schultz-Coulon[11], F. Sefkow[37], A. Semenov[24], V. Shekelyan[26], I. Sheviakov[25], L.N. Shtarkov[25], G. Siegmon[16], Y. Sirois[28], T. Sloan[18], P. Smirnov[25], M. Smith[19], V. Solochenko[24], Y. Soloviev[25], L. Sonnenschein[2], V. Spaskov[9], A. Specka[28], H. Spitzer[12], F. Squinabol[27], R. Stamen[8], P. Steffen[11], R. Steinberg[2], J. Steinhart[12], B. Stella[32], A. Stellberger[15], J. Stiewe[15], U. Straumann[14], W. Struczinski[2], J.P. Sutton[3], M. Swart[15], S. Tapprogge[15], M. Taševský[30], V. Tchernyshov[24], S. Tchetchelnitski[24], J. Theissen[2], G. Thompson[20], P.D. Thompson[3], N. Tobien[11], R. Todenhagen[13], D. Traynor[20], P. Truöl[37], G. Tsipolitis[36], J. Turnau[6], E. Tzamariudaki[26], S. Udluft[26], A. Usik[25], S. Valkár[31], A. Valkárová[31], C. Vallée[23], P. Van Esch[4], A. Van Haecke[10], P. Van Mechelen[4], Y. Vazdik[25], G. Villet[10], K. Wacker[8], R. Wallny[14], T. Walter[37], B. Waugh[22], G. Weber[12], M. Weber[15], D. Wegener[8], A. Wegner[26], T. Wengler[14], M. Werner[14], L.R. West[3], S. Wiesand[34], T. Wilksen[11], S. Willard[7], M. Winde[35], G.-G. Winter[11], Ch. Wissing[8], C. Wittek[12], E. Wittmann[13], M. Wobisch[2], H. Wollatz[11], E. Wünsch[11], J. Žáček[31], J. Zálešák[31], Z. Zhang[27], A. Zhokin[24], P. Zini[29], F. Zomer[27], J. Zsembery[10] and M. zur Nedden[37]

[1] I. Physikalisches Institut der RWTH, Aachen, Germany[a]
[2] III. Physikalisches Institut der RWTH, Aachen, Germany[a]
[3] School of Physics and Space Research, University of Birmingham, Birmingham, UK[b]
[4] Inter-University Institute for High Energies ULB-VUB, Brussels; Universitaire Instelling Antwerpen, Wilrijk; Belgium[c]
[5] Rutherford Appleton Laboratory, Chilton, Didcot, UK[b]
[6] Institute for Nuclear Physics, Cracow, Poland[d]
[7] Physics Department and IIRPA, University of California, Davis, California, USA[e]
[8] Institut für Physik, Universität Dortmund, Dortmund, Germany[a]
[9] Joint Institute for Nuclear Research, Dubna, Russia
[10] DSM/DAPNIA, CEA/Saclay, Gif-sur-Yvette, France
[11] DESY, Hamburg, Germany[a]
[12] II. Institut für Experimentalphysik, Universität Hamburg, Hamburg, Germany[a]
[13] Max-Planck-Institut für Kernphysik, Heidelberg, Germany[a]
[14] Physikalisches Institut, Universität Heidelberg, Heidelberg, Germany[a]
[15] Institut für Hochenergiephysik, Universität Heidelberg, Heidelberg, Germany[a]
[16] Institut für experimentelle und angewandte Physik, Universität Kiel, Kiel, Germany[a]
[17] Institute of Experimental Physics, Slovak Academy of Sciences, Košice, Slovak Republic[f,j]
[18] School of Physics and Chemistry, University of Lancaster, Lancaster, UK[b]
[19] Department of Physics, University of Liverpool, Liverpool, UK[b]
[20] Queen Mary and Westfield College, London, UK[b]
[21] Physics Department, University of Lund, Lund, Sweden[g]
[22] Department of Physics and Astronomy, University of Manchester, Manchester, UK[b]
[23] CPPM, Université d'Aix-Marseille II, IN2P3-CNRS, Marseille, France
[24] Institute for Theoretical and Experimental Physics, Moscow, Russia
[25] Lebedev Physical Institute, Moscow, Russia[f,k]
[26] Max-Planck-Institut für Physik, München, Germany[a]
[27] LAL, Université de Paris-Sud, IN2P3-CNRS, Orsay, France
[28] LPNHE, École Polytechnique, IN2P3-CNRS, Palaiseau, France
[29] LPNHE, Universités Paris VI and VII, IN2P3-CNRS, Paris, France
[30] Institute of Physics, Academy of Sciences of the Czech Republic, Praha, Czech Republic[f,h]

[31] Nuclear Center, Charles University, Praha, Czech Republic[f,h]
[32] INFN Roma 1 and Dipartimento di Fisica, Università Roma 3, Roma, Italy
[33] Paul Scherrer Institut, Villigen, Switzerland
[34] Fachbereich Physik, Bergische Universität Gesamthochschule Wuppertal, Wuppertal, Germany[a]
[35] DESY, Institut für Hochenergiephysik, Zeuthen, Germany[a]
[36] Institut für Teilchenphysik, ETH, Zürich, Switzerland[i]
[37] Physik-Institut der Universität Zürich, Zürich, Switzerland[i]
[38] Institut für Physik, Humboldt-Universität, Berlin, Germany[a]
[39] Rechenzentrum, Bergische Universität Gesamthochschule Wuppertal, Wuppertal, Germany[a]
[40] Vistor from Yerevan Physics Institute, Armenia
[41] Foundation for Polish Science fellow
[42] Institut für Experimentelle Kernphysik, Universität Karlsruhe, Karlsruhe, Germany
[43] Dept. Fís. Ap. CINVESTAV, Mérida, Yucatán, México

[a] Supported by the Bundesministerium für Bildung, Wissenschaft, Forschung und Technologie, FRG, under contract numbers 7AC17P, 7AC47P, 7DO55P, 7HH17I, 7HH27P, 7HD17P, 7HD27P, 7KI17I, 6MP17I and 7WT87P
[b] Supported by the UK Particle Physics and Astronomy Research Council, and formerly by the UK Science and Engineering Research Council
[c] Supported by FNRS-FWO, IISN-IIKW
[d] Partially supported by the Polish State Committee for Scientific Research, grant no. 115/E-343/SPUB/P03/002/97 and grant no. 2P03B 055 13
[e] Supported in part by US DOE grant DE F603 91ER40674
[f] Supported by the Deutsche Forschungsgemeinschaft
[g] Supported by the Swedish Natural Science Research Council
[h] Supported by GA ČR grant no. 202/96/0214, GA AV ČR grant no. A1010821 and GA UK grant no. 177
[i] Supported by the Swiss National Science Foundation
[j] Supported by VEGA SR grant no. 2/5167/98
[k] Supported by Russian Foundation for Basic Research grant no. 96-02-00019

1 Introduction

A sizeable fraction of the final states produced in high energy collisions shows the characteristic feature of large amounts of hadronic energy in small angular regions. These collimated sprays of hadrons (called jets) are the observable signals of underlying short distance processes and are considered to be the footprints of the underlying partonic final states. Quantitative studies of jet production require a precise jet definition, which is given by a jet finding algorithm.

Jets so defined exhibit an internal structure which is sensitive to the mechanism by which a complex aggregate of observable hadrons evolves from a hard process. The understanding of this mechanism involves higher orders of the strong coupling constant in perturbation theory as well as non-perturbative contributions. This is a challenging task for theory. Recently, for some specific hadronic final state quantities, encouraging results have been obtained by exploiting the characteristic power behaviour of non-perturbative effects and by analytical, approximate calculations of perturbative QCD parton evolution down to the semi-soft regime [1, 2]. Furthermore, since jet production rates are used to test the predictions of perturbative QCD, the understanding of their detailed properties and internal structure is an important prerequisite.

The internal structure of jets has been studied in e^+e^- [3] and in hadron-hadron collisions [4]. At the $e^{\pm}p$ collider HERA, these investigations can be performed in photoproduction ($Q^2 \approx 0\ \mathrm{GeV}^2$) and in deep-inelastic scattering (DIS) at large squared four momentum transfers Q^2. In a previous publication we have measured the E_T dependence of the jet width [5] in photoproduction. Recently, the ZEUS collaboration has investigated jet shapes in photoproduction [6] and in DIS at $Q^2 > 100\ \mathrm{GeV}^2$ [7]. Both analyses are carried out in the laboratory frame. This means that for DIS at high Q^2 mostly events with only one jet enter the analysis.

The hadronization of the current jet in deep-inelastic scattering in the Breit frame has already been studied with event shape variables [8], charged particle multiplicities and fragmentation functions [9]. In this paper we take the first steps towards a complete understanding of jet properties in DIS. We analyse the hadronization of jets in multijet production in the Breit frame. The Breit frame, where the virtual photon interacts head-on with the proton, has been chosen in this analysis because here the produced transverse[1] energy, $E_{T,\mathrm{Breit}}$, directly reflects the hardness of the underlying QCD process. We present measurements of internal jet structure in a sample of inclusive dijet events with transverse jet energies of $E_{T,\mathrm{Breit}} > 5$ GeV, $10 < Q^2 \lesssim 120\,\mathrm{GeV}^2$ and $2 \cdot 10^{-4} \lesssim x_{\mathrm{Bj}} \lesssim 8 \cdot 10^{-3}$. This is the $E_{T,\mathrm{Breit}}$ range where jet cross section measurements are currently performed at HERA and compared to perturbative QCD calculations (e.g. [10, 11]). The analysis is based on data taken in 1994 with the H1 detector at HERA when 27.5 GeV positrons collided with 820 GeV protons. The data correspond to an integrated luminosity of $\mathcal{L}_{\mathrm{int}} \simeq 2\,\mathrm{pb}^{-1}$.

Jets are defined in the Breit frame by $k_\perp$ and cone jet algorithms. Two observables, jet shapes and, for the first time, subjet multiplicities, are studied. The jet shape measures the radial distribution of the transverse jet energy around the jet axis. For the $k_\perp$ cluster algorithm we have also measured the multiplicity of subjets, resolved at a resolution scale which is a

[1] transverse with respect to the z-axis which is given by the axis of the virtual photon and the proton.

fraction of the jet's transverse energy. Both observables are presented for different ranges of the transverse jet energy and the pseudo-rapidity[2] of the jets in the Breit frame.

The paper is organized as follows. Section 2 gives a brief description of the H1 detector. In section 3 we introduce the jet algorithms used in the analysis and give the definition of the measured observables in section 4. In section 5 we give a short description of the QCD models which are used for the correction of the data and to which the results are later compared (in section 9). The data selection and the correction procedure are described in sections 6 and 7 and the results are discussed in section 8.

2 The H1 Detector

A detailed description of the H1 detector can be found elsewhere [12]. Here we briefly introduce the detector components relevant for this analysis: the liquid argon (LAr) calorimeter [13], the backward lead-scintillator calorimeter (BEMC) [14], and the tracking chamber system [15].

The hadronic energy flow is mainly measured by the LAr calorimeter extending over the polar angular range $4.4^\circ < \theta < 154^\circ$ with full azimuthal coverage. The polar angle θ is defined with respect to the proton beam direction ($+z$ axis). The LAr calorimeter consists of an electromagnetic section ($20 - 30$ radiation lengths) with lead absorbers and a hadronic section with steel absorbers. The total depth of both calorimeters varies between 4.5 and 8 interaction lengths. Test beam measurements of the LAr calorimeter modules show an energy resolution of $\sigma_E/E \approx 0.50/\sqrt{E\,[\mathrm{GeV}]} \oplus 0.02$ for charged pions [16]. The absolute scale of the hadronic energy is known for the present data sample to 4%.

The scattered positron is detected by the BEMC with a depth of 22.5 radiation lengths covering the backward region of the detector, $155^\circ < \theta < 176^\circ$. The electromagnetic energy scale is known to an accuracy of 1%.

The calorimeters are surrounded by a superconducting solenoid providing a uniform magnetic field of 1.15 T parallel to the beam axis in the tracking region.

Charged particle tracks are measured in two concentric jet drift chamber modules (CJC), covering the polar angular range $15^\circ < \theta < 165^\circ$. The forward tracking detector covers $7^\circ < \theta < 25^\circ$ and consists of drift chambers with alternating planes of parallel wires and others with wires in the radial direction. A backward proportional chamber (BPC) with an angular acceptance of $151^\circ < \theta < 174.5^\circ$ improves the identification of the scattered positron. The spatial resolution for reconstructed BPC hits is about 1.5 mm in the plane perpendicular to the beam axis.

3 Jet Definitions

The jet algorithms used in this analysis are applied to the particles boosted into the Breit frame. Particle refers here either to an energy deposit in the detector (see section 6), to a stable hadron

[2]The pseudo-rapidity η is defined as $\eta \equiv -\ln(\tan\theta/2)$ where θ is the polar angle with respect to the proton direction. This definition is chosen in both the laboratory frame and the Breit frame.

or a parton in a QCD model calculation. In all cases the scattered positron is excluded. The Breit frame is defined by $\vec{q} + 2x_{\mathrm{Bj}}\vec{P} = 0$, where $\vec{q}$ and $\vec{P}$ are the momenta of the exchanged boson and the incoming proton. The z-axis is defined as the direction of the incoming proton.

In the following analysis we use two different jet definitions: a cone algorithm and a $k_\perp$ cluster algorithm. Both jet definitions are invariant under boosts along the z-direction. The recombination of particles is carried out in the E_T recombination scheme, which is based on transverse energies E_T, pseudo-rapidities η and azimuthal angles ϕ of the particles. The transverse energy and the direction of a jet are defined by

$$E_{T,\mathrm{jet}} = \sum_i E_{T,i}, \qquad \eta_{\mathrm{jet}} = \frac{\sum_i E_{T,i}\,\eta_i}{\sum_i E_{T,i}}, \qquad \phi_{\mathrm{jet}} = \frac{\sum_i E_{T,i}\,\phi_i}{\sum_i E_{T,i}}, \tag{1}$$

where the sums run over all particles i assigned to the jet[3].

3.1 Cone Algorithm

Based on the original proposal of Sterman and Weinberg [17] many different implementations of cone algorithms have been developed. While the basic idea of the cone algorithm is simple and very intuitive, an operational definition is non-trivial. The resulting jet cross sections depend on how the algorithm treats the choice of jet initiators and configurations of overlapping jet cones. It has repeatedly been pointed out that many definitions of cone algorithms are not infrared and/or collinear safe [18, 19].

In this analysis we use the definition implemented in the algorithm PXCONE [20] which does not suffer from the problems discussed in [18, 19]. This definition, which corresponds closely to the Snowmass proposal [21] and to the algorithm used in the CDF experiment [22], is also used by the OPAL collaboration [23].

Particles are assigned to jets based on their spatial distance R in pseudo-rapidity and azimuth space ($R^2 = \Delta\eta^2 + \Delta\phi^2$). The algorithm operates as follows:

1. Each particle is considered as a seed of a jet, for which steps 2-4 are performed.
2. The jet momentum is calculated from all particles within a cone of radius R_0 around the seed direction using eq. (1).
3. If the jet direction differs from the seed direction, the jet direction is taken as the new seed direction and step 2 is repeated.
4. When the jet direction is stable the jet is stored in the list of "protojets" (if it is not identical with a protojet already found).
5. The steps 2 to 4 are repeated for all midpoints of pairs of protojets as seed directions[4]. This leads to the infrared safety of the procedure [19].

[3] All particles are considered massless by setting $E_i = |\vec{p}_i|$.

[4] In practice it is sufficient to do this only for pairs of protojets with a distance between R_0 and $2\,R_0$.

6. Protojets with transverse energies of $E_{T,\mathrm{jet}} < \epsilon$ are removed from the list. The cut-off parameter ϵ specifies below which transverse energies protojets are not considered in the overlap treatment (steps 7-8).

7. All remaining protojets that have more than a fraction f of their transverse energy contained in a protojet of higher transverse energy are deleted.

8. All particles that are contained in more than one protojet are assigned to the protojet whose center is nearest in (η, ϕ).

9. The jet momenta are recalculated using eq. (1). All protojets with $E_{T,\mathrm{jet}} < \epsilon$ are deleted and the remaining ones are called jets.

The jets with the highest transverse energies are considered in the analysis. Due to the reassignment of particles to jets and the recalculation of the jet axis (steps 7, 8) it may happen that single particles within a jet have a distance larger than R_0 to the jet axis. This analysis is made with the parameter settings $\epsilon = 5\,\mathrm{GeV}$, $f = 0.75$ and a cone radius of $R_0 = 1.0$.

3.2 Inclusive $k_\perp$ Algorithm

The ambiguities that occur for cone jet definitions (choice of seeds, overlapping cones) are avoided in cluster algorithms which successively recombine particles to jets. One definition of such an algorithm (proposed in [24] and implemented in the KTCLUS algorithm [25]) has properties very similar to cone algorithms. As in the cone algorithm the clustering procedure is based on the longitudinally boost-invariant quantities $E_T, \Delta\eta, \Delta\phi$. The minimum of all distances between particles is determined and either the corresponding pairs of particles are merged into pseudo-particles or single (pseudo-) particles are declared as jets. This process is iterated until no particles are left:

1. We start with a list of all particles and an empty list of jets.

2. For each particle i as well as for each pair of particles (i, j) the distances d_i and d_{ij} are calculated

$$d_i = E_{T,i}^2\, R_0^2 \quad \text{and} \quad d_{ij} = \min(E_{T,i}^2, E_{T,j}^2)\, R_{ij}^2 \quad \text{with} \quad R_{ij}^2 = \Delta\eta_{ij}^2 + \Delta\phi_{ij}^2\,. \qquad (2)$$

3. The smallest value of all the d_i and d_{ij} is labeled $d_{\min}$.

4. If $d_{\min}$ belongs to the set of d_{ij}, the particles i and j are merged into a new particle using the recombination prescription in eq. (1) and removed from the list of particles.

5. If $d_{\min}$ belongs to the set of d_i, the particle i is removed from the list of particles and added to the list of jets.

6. When no particles are left (i.e. all particles are included in jets) the procedure is finished.

The last jets that entered the list are the ones with highest transverse energies. These jets are considered in the analysis. This jet definition implies that particles with $R_{ij} < R_0$ are subsequently merged, so that all final jets are separated by distances $R_{ij} > R_0$. It is still possible that particles inside a jet have a distance $R_{ij} > R_0$ to the jet axis and that particles with $R_{ij} < R_0$ are not part of the jet. The parameter R_0 is set to $R_0 = 1.0$.

4 The Observables

Two observables of internal jet structure are investigated in this analysis. They are sensitive to different aspects of jet broadening.

The jet shapes are studied for the cone and the $k_\perp$ algorithm. This observable measures the radial distribution of the transverse jet energy only and is affected by hard and by soft processes over the whole radial range.

A natural choice for studying the internal structure of jets with the $k_\perp$ cluster algorithm is the multiplicity of subjets, resolved at a resolution scale which is a fraction of the jet's transverse energy. These subjet multiplicities are sensitive to more local structures of relative transverse momentum within a jet. Here the perturbative and the non-perturbative contributions are better separated. While at larger values of the resolution parameter perturbative contributions dominate, at smaller values non-perturbative contributions become increasingly important.

4.1 The Jet Shape

The jet shape $\Psi(r)$ is defined as the fractional transverse jet energy contained in a subcone of radius r concentric with the jet axis, averaged over all considered jets in the event sample

$$\Psi(r) \equiv \frac{1}{N_{\text{jets}}} \sum_{\text{jets}} \frac{E_T(r)}{E_{T,\text{jet}}}, \tag{3}$$

where N_{jets} is the total number of these jets. As proposed in [19], only particles assigned by the jet algorithm to the jet are considered.

Usually the denominator in the definition of Ψ is given by the summed E_T of all particles within a radius R_0 to the jet axis. This means that $\Psi(r/R_0 = 1) = 1$. In our definition (3) of Ψ the denominator is given by the transverse energy of the jet. Since neither for the cone nor for the $k_\perp$ definition are all particles necessarily assigned to a jet within a radius of $r/R_0 < 1$ to the jet axis, $\Psi(r/R_0 = 1)$ is not constrained to have the value of one. With this choice of our observable we are also sensitive to the amount of transverse jet energy outside the radius R_0.

4.2 Subjet Multiplicities

For each jet in the sample the clustering procedure is repeated for all particles assigned to the jet. The clustering is stopped when the distances y_{ij} between all particles i, j are above some cut-off y_{cut}

$$y_{ij} \;=\; \frac{\min(E_{T,i}^2, E_{T,j}^2)}{E_{T,\text{jet}}^2} \;\frac{\left(\Delta\eta_{ij}^2 + \Delta\phi_{ij}^2\right)}{R_0^2} \;>\; y_{\text{cut}} \tag{4}$$

and the remaining (pseudo-)particles are called subjets. The parameter y_{cut} defines the minimal relative transverse energy between subjets inside the jet and thus determines the extent to which the internal jet structure is resolved. From this definition it follows that for $y_{\text{cut}} > 0.25$ no subjet is resolved (therefore the number of subjets is one), while for $y_{\text{cut}} \to 0$ every particle in the jet is a subjet. The observable that is studied in this analysis is the average number of subjets for a given value of the resolution parameter, for values $y_{\text{cut}} \geq 10^{-3}$.

5 QCD Models

A simulation of the detailed properties of the hadronic final state is available in the form of Monte Carlo event generators. They include the matrix element of the hard subprocess in first order of the strong coupling constant α_s, approximations of higher order QCD radiation effects, and a model to describe the non-perturbative transition from partons to hadrons.

The LEPTO Monte Carlo [26] incorporates the $\mathcal{O}(\alpha_s)$ QCD matrix element and takes higher order parton emissions to all orders in α_s approximately into account using the concept of parton showers [27] based on the leading logarithm DGLAP equations [28]. QCD radiation can occur before and after the hard subprocess. The formation of hadrons is performed using the LUND string model [29] implemented in JETSET [30].

The HERWIG Monte Carlo [31] also includes the $\mathcal{O}(\alpha_s)$ QCD matrix element, but uses another implementation of the parton shower cascade which takes coherence effects fully into account. The hadronization is simulated with the cluster fragmentation model [32].

In ARIADNE [33] gluon emissions are treated by the colour dipole model [34] assuming a chain of independently radiating dipoles spanned by colour connected partons. The first emission in the cascade is corrected to reproduce the matrix element to first order in α_s [35].

DJANGO [36] provides an interface between the event generators LEPTO or ARIADNE and HERACLES [37] which makes it possible to include $\mathcal{O}(\alpha)$ QED corrections at the lepton line.

6 Data Selection

The analysis is based on H1 data taken in 1994 corresponding to an integrated luminosity of $\mathcal{L}_{int} \simeq 2\,\mathrm{pb}^{-1}$. The event selection closely follows that described in a previous publication [10]. DIS events are selected where the scattered positron is measured in the acceptance region of the BEMC at energies where trigger efficiencies are approximately 100 %. To ensure a good identification of the scattered positron and to suppress background from misidentified photoproduction events the following cuts are applied:

- The cluster of the positron candidate must have an energy-weighted mean transverse radius below 5 cm.
- A reconstructed BPC hit within 5 cm of the straight line connecting the shower center with the event vertex is required.
- The z position of the reconstructed event vertex must be within ± 30 cm of the nominal position.
- A cut on $35\,\mathrm{GeV} < \sum(E - p_z) < 70\,\mathrm{GeV}$ is applied, where the sum runs over all energy deposits in the calorimeter. In neutral current DIS events without undetected photon radiation the quantity $\sum(E - p_z)$ is expected to be equal to twice the energy of the initial state positron. This cut reduces the contribution from photoproduction events as well as events where hard photons are radiated collinear to the incoming positron.

The event kinematics are calculated from the polar angle θ_{el} and the energy E'_{el} of the scattered positron via $Q^2_{el} = 2\,E_0\,E'_{el}\,(1+\cos\theta_{el})$, $y_{el} = 1 - E'_{el}/(2\,E_0)(1-\cos\theta_{el})$ and $x_{\rm Bj} = Q^2/(sy)$. E_0 denotes the energy of the incoming positron and s the ep centre-of-mass energy squared. Events are only accepted, if $E'_{el} > 11$ GeV, $156^\circ < \theta_{el} < 173^\circ$, $Q^2 > 10\,{\rm GeV}^2$ and $y > 0.15$. The resulting kinematic range is $10 < Q^2 \lesssim 120\,{\rm GeV}^2$ and $2\cdot 10^{-4} \lesssim x_{\rm Bj} \lesssim 8\cdot 10^{-3}$.

Jets are defined by the algorithms described in section 3. The input for the jet algorithms consists of a combination of energy clusters from the calorimeter and track momenta measured in the central and forward trackers (as described in [10]). While all energy clusters are considered, the four momentum of each single track is only allowed to contribute up to a momentum of $350\,{\rm MeV}$. This procedure partly compensates for energy losses in the calorimeter due to dead material and noise thresholds. It reduces the dependence of the jet finding efficiency on the pseudo-rapidity of the jet and improves the reconstruction of the transverse jet energy [38].

The objects from tracking and calorimeter information are boosted to the Breit frame where the jet algorithms are applied. We select events with at least two identified jets with transverse energies of $E_{T,{\rm Breit}} > 5\,{\rm GeV}$ in $-1 < \eta_{\rm jet,lab} < 2$. The two jets with the highest $E_{T,{\rm Breit}}$ are considered in the analysis. The event sample for the inclusive $k_\perp$ algorithm (the cone algorithm) consists of 2045 (2657) dijet events.

7 Correction of the Data

The data are corrected for detector effects and QED radiation from the lepton. The detector response is determined using events from Monte Carlo event generators that were subjected to a detailed simulation of the H1 detector. The following event generators are used: ARIADNE interfaced in DJANGO (with and without the inclusion of QED corrections) and LEPTO. Both generators give a good description of the kinematic variables of the inclusive DIS data sample as well as of the angular and transverse energy distributions of the jets [39]. We also observe a reasonable description of the observables introduced in section 4 (see section 9).

The measured data points are corrected bin-by-bin for detector effects. Using the generated event samples, the correction factor for each bin is determined as the ratio of the generated value of the observable and the value that is reconstructed after detector simulation. These correction factors are independent of the inclusion of QED radiation effects as included in DJANGO. Their dependence on details of the modeling of the hadronic final state is taken into account by considering the difference between the correction factors from ARIADNE and LEPTO as systematic uncertainty.

For the $k_\perp$ (cone) algorithm the corrections for $\Psi(r)$ are below $10\,\%$ ($13\,\%$) for subcone radii $r > 0.3$ and always below $27\,\%$ ($23\,\%$). The corrections for $\langle N_{\rm subjet}(y_{\rm cut})\rangle$ are always below 7%. The correction factors from both QCD models are in good agreement (they differ typically by not more than $2\,\%$) for the jet shapes as well as for the subjet multiplicities [39]. The final correction factors are taken to be the mean values of the two models, taking the spread as the error. In addition we have varied the calibration of the hadronic energy scale in the data sample in the range of $\pm 4\%$ around the nominal value. The error is estimated as the maximal deviation

from the results at the nominal value. For all observables it is at most 5%. The overall systematic error is calculated by adding the errors from the model dependence and from the uncertainty of the hadronic energy scale in quadrature. In all figures the statistical and systematic errors are added in quadrature. Since each jet enters in all bins of a distribution, all errors are correlated.

The background from misidentified photoproduction events is estimated with a sample of photoproduction events generated with PHOJET [40] and is found to be negligible.

8 Results

The jet shape and the subjet multiplicity are presented as functions of quantities directly related to the single jets, namely the transverse jet energy ($E_{T,\text{Breit}}$) and the pseudo-rapidity (η_{Breit}) in the Breit frame. We also investigated whether the observables depend on the event kinematics. The jet shapes and subjet multiplicities were compared for two bins of Q^2 ($Q^2 < 20\,\text{GeV}^2$ and $Q^2 > 20\,\text{GeV}^2$) and x_{Bj} ($x_{\text{Bj}} < 8 \cdot 10^{-4}$ and $x_{\text{Bj}} > 8 \cdot 10^{-4}$) respectively. No dependence on Q^2 and x_{Bj} has been observed.

8.1 Jet Shapes

The radial dependence of the jet shape $\Psi(r)$ for the $k_\perp$ algorithm is shown in Fig. 1 in different ranges of the pseudo-rapidity in the Breit frame. The results for jets of transverse energies $5 < E_{T,\text{Breit}} < 8\,\text{GeV}$ and $E_{T,\text{Breit}} > 8\,\text{GeV}$ are superimposed. The jet shape $\Psi(r)$ increases faster with r for jets at larger transverse energies, indicating that these jets are more collimated. The same tendency is seen for the jets defined by the cone algorithm which are compared to the jets found by the $k_\perp$ algorithm in Fig. 2. For both jet definitions we also observe a dependence of the jet shape on the pseudo-rapidity of the jets. Jets towards the proton direction (at larger values of η_{Breit}) are broader than jets towards the photon direction (smaller η_{Breit}). In the region where the jets are most collimated ($E_{T,\text{Breit}} > 8\,\text{GeV}$ and $\eta_{\text{Breit}} < 2.2$), very similar jet shapes are observed for the $k_\perp$ and cone algorithms. The broadening of the jets for smaller $E_{T,\text{Breit}}$ and larger η_{Breit} is more pronounced for the cone jet definition.

Recently jet shapes have been measured in dijet production in photon-photon collisions [41] for jets defined by a cone algorithm at transverse energies comparable to those presented here. The jet shapes in photon-photon collisions (where no η dependence is observed) are very similar to those measured in DIS in the Breit frame at $\eta_{\text{Breit}} < 1.5$.

8.2 Subjet Multiplicities

The subjet multiplicities for the $k_\perp$ algorithm are displayed in Fig. 3. The average number of subjets $\langle N_{\text{subjet}}(y_{\text{cut}})\rangle$ as a function of the subjet resolution parameter at $y_{\text{cut}} \geq 10^{-3}$ is plotted. Towards smaller values of y_{cut}, an increasing number of jet fragments with smaller relative transverse momenta is resolved. The number of subjets at a given value of y_{cut} reflects the

amount of relative transverse momentum with respect to the jet axis. The subjet multiplicity is therefore a measure of the broadness of the jet.

At $y_{\rm cut} = 10^{-3}$ a jet is on average resolved into $4.1 - 4.6$ subjets, depending on $E_{T,\rm Breit}$ and $\eta_{\rm Breit}$ of the jet[5]. For almost all values of $y_{\rm cut}$ the subjet multiplicity is larger for jets at smaller $E_{T,\rm Breit}$ and larger $\eta_{\rm Breit}$, indicating broader jets.

A summary of the results for both observables is given in Fig. 4. Here the $E_{T,\rm Breit}$ and the $\eta_{\rm Breit}$ dependence of the jet shape and the average number of subjets are shown at an intermediate value of the resolution parameter (jet shape: $r = 0.5$ and subjet multiplicity: $y_{\rm cut} = 10^{-2}$).

Although the subjet multiplicities are sensitive to the jet broadening in a different way than the jet shapes, consistent conclusions can be drawn for both measurements. The jet broadening depends on both the transverse jet energy as well as the pseudo-rapidity in the Breit frame. While the pseudo-rapidity dependence is most pronounced at smaller transverse jet energy, the transverse energy dependence is stronger in the forward region (at larger pseudo-rapidities).

9 Comparison with QCD Model Predictions

The predictions of different QCD models are compared in Fig. 5 to the jet shapes measured for the $k_\perp$ algorithm. The models LEPTO, ARIADNE and HERWIG all show $E_{T,\rm Breit}$ and $\eta_{\rm Breit}$ dependences similar to that seen in the data. LEPTO gives the best description of the measured shapes for $\eta_{\rm Breit} < 2.2$ while at $\eta_{\rm Breit} > 2.2$ the predicted jet shapes are too broad. A reasonable description is also obtained by the ARIADNE model except for jets at smaller pseudo-rapidities where the jet shapes have the tendency to be too narrow. For the HERWIG model the jet shapes are narrower than those in the data in all $E_{T,\rm Breit}$ and $\eta_{\rm Breit}$ regions. The same observations as above are made when comparing these QCD models with the subjet multiplicities and with the jet shapes for the cone algorithm (not shown here).

In QCD models the evolution of a jet is described by perturbative contributions (radiation of partons) and non-perturbative contributions (hadronization). Studies based on the LEPTO and HERWIG parton shower models show that all observables studied in this analysis are strongly influenced by hadronization. This process has the largest impact on the jet broadening in our kinematic region (Fig. 6). Basic characteristics of the perturbative contributions are however still visible after hadronization. The model prediction suggests that the large difference between quark and gluon-initiated jets before hadronization survives the hadronization process. This especially applies to jets with large transverse energies [39].

Fig. 6 shows the jet shapes and the subjet multiplicities as predicted by the LEPTO parton shower model for the $k_\perp$ algorithm, separately for quark and gluon jets at $E_{T,\rm Breit} > 8\,\rm GeV$ and $\eta_{\rm Breit} < 1.5$. Gluon jets are broader than quark jets. The same prediction is obtained by the HERWIG parton shower model. Although the jets in HERWIG are slightly narrower, the differences between gluon and quark jets are equally large. In the phase space considered here, LEPTO and HERWIG (in agreement with next-to-leading order calculations) predict a fraction

[5]On average the jets in the data (as in the simulated events) consist of eleven calorimetric energy clusters. For the LEPTO generator this is also approximately the average multiplicity of stable particles inside the jets.

of approximately 80% photon-gluon fusion events with two quarks in the partonic final state. The jet samples of these models are therefore dominated by quark jets. Both model predictions for the jet shapes and the subjet multiplicities therefore mainly reflect the properties of the quark jets as can be seen in Fig. 6. These predictions give a reasonable description of the data. Thus, we conclude, that the jets we observe are consistent with being mainly initiated by quarks.

10 Summary

Measurements of internal jet structure in dijet events in deep-inelastic scattering in the kinematic domain $10 < Q^2 \lesssim 120\,\mathrm{GeV}^2$ and $2 \cdot 10^{-4} \lesssim x_{\mathrm{Bj}} \lesssim 8 \cdot 10^{-3}$ have been presented. Jet shapes and subjet multiplicities have been studied for jets of transverse energies $E_{T,\mathrm{Breit}} > 5\,\mathrm{GeV}$ defined by $k_\perp$ and cone jet algorithms in the Breit frame.

The radial dependence of the jet shape and the dependence of the average number of subjets on the subjet resolution parameter y_{cut} are both sensitive to different aspects of jet broadening. For both observables a dependence of the jet broadness on the transverse energy $E_{T,\mathrm{Breit}}$ and on the pseudo-rapidity in the Breit frame η_{Breit} is seen. With increasing $E_{T,\mathrm{Breit}}$ jets are narrower. Jets of the same $E_{T,\mathrm{Breit}}$ become broader towards the proton direction. This effect is more pronounced at lower $E_{T,\mathrm{Breit}}$.

At lower $E_{T,\mathrm{Breit}}$ jets defined by the $k_\perp$ algorithm are more collimated than jets defined by the cone algorithm, while at higher $E_{T,\mathrm{Breit}}$ both algorithms produce very similar jets.

The QCD models LEPTO, ARIADNE and HERWIG roughly reproduce the dependence of the jet shape and the subjet multiplicities on $E_{T,\mathrm{Breit}}$ and η_{Breit} as seen in the data. LEPTO has a tendency to produce broader jets in the proton direction than measured. HERWIG and ARIADNE produce jets which are too collimated especially at higher transverse energies. We have reported earlier that in the same kinematic domain the predicted jet rates from LEPTO and HERWIG are about a factor of two below the data [10]. Since these models are able to reproduce the internal jet structure, this failure must be largely connected to an inadequate modeling of the underlying hard partonic subprocess.

According to the parton shower models LEPTO and HERWIG, quark and gluon initiated jets differ both at the parton and at the hadron level. Both models predict that the jet sample is dominated by quark initiated jets. Since these models describe our data, we conclude that the observed jet structures are compatible with those of quark initiated jets.

11 Acknowledgments

We are grateful to the HERA machine group whose outstanding efforts have made and continue to make this experiment possible. We thank the engineers and technicians for their work in constructing and now maintaining the H1 detector, our funding agencies for financial support, the DESY technical stuff for continual assistance, and the DESY directorate for the hospitality which they extend to the non-DESY members of the collaboration.

References

[1] B.R. Webber, Phys. Lett. 339 (1994) 148;
Yu.L. Dokshitzer and B.R. Webber, Phys. Lett. B 352 (1995) 451;
M. Dasgupta and B.R. Webber, Eur. Phys. J. C 1 (1998) 539.

[2] V. Khoze and W. Ochs, Int. J. Mod. Phys. A 12 (1997) 2949;
S. Lupia, W. Ochs, Phys. Lett. B 418 (1998) 214.

[3] OPAL Collab., R. Akers et al., Z. Phys. C 63 (1994) 197; Z. Phys. C 68 (1995) 179; Z. Phys. C 69 (1996) 543;
DELPHI Collab., P. Abreu et al., CERN-EP/98-24;
P. Mättig, Phys. Rep. 177 (1989) 141.

[4] D0 Collab., S. Abachi et al., Phys. Lett. B 357 (1995) 500;
CDF Collab., F. Abe et al., Phys. Rev. Lett. 70 (1993) 713.

[5] H1 Collab., S. Aid et al., Z. Phys. C 70 (1996) 17.

[6] ZEUS Collab., J.Breitweg et al. , Europ. Phys. J. C 2 (1998) 61.

[7] ZEUS Collab., J. Breitweg et al., DESY 98-038, Hamburg, Germany (1998), subm. to Eur. Phys. J.

[8] H1 Collab., C. Adloff et al., Phys. Lett. B 406 (1997) 256.

[9] H1 Collab., C. Adloff et al., Nucl. Phys. B 504 (1997) 3.

[10] H1 Collab., C. Adloff et al., DESY-98-076 Hamburg, Germany (1998), submitted to Eur. Phys. J. C.

[11] H1 Collab., C. Adloff et al., DESY-98-205 Hamburg, Germany (1998), submitted to Eur. Phys. J. C.

[12] H1 Collab., I. Abt et al., Nucl. Instr. and Meth. A 386 (1997) 310 and 348.

[13] H1 Calorimeter Group, B. Andrieu et al., Nucl. Instr. and Meth. A 336 (1993) 460.

[14] H1 BEMC Group, J. Bán et al., Nucl. Instr. and Meth. A 372 (1996) 399.

[15] J. Bürger et al., Nucl. Inst. Meth. A 279 (1989) 217;
H1 FTD Group, S. Burke et al., Nucl. Inst. Meth. A 313 (1996) 373.

[16] H1 Calorimeter Group, B. Andrieu et al., Nucl. Instr. and Meth. A 372 (1996) 399.

[17] G. Sterman and S. Weinberg, Phys. Rev. Lett. 39 (1977) 1436.

[18] D.E. Soper, in: Recontres de Moriond, Les Arc, France (1997) and hep-ph/9706320.

[19] M.H. Seymour, in: Les Rencontres de la Vallée d'Aoste, La Thuile, France (1997) and Nucl. Phys. B 513 (1998) 269.

[20] L.A. del Pozo, PhD Thesis University of Cambridge, Cambridge, England (1993) RALT-002.

[21] J. Huth et al., Proceedings of the Summer Study on High Energy Physics, Snowmass, Colorado (1990) 134.

[22] CDF Collab., F. Abe et al., Phys. Rev. D 45 (1992) 1448.

[23] OPAL Collab., R. Akers et al., Z. Phys. C 63 (1994) 197 and Z. Phys. C 68 (1995) 179.

[24] S.D. Ellis and D.E. Soper, Phys. Rev. D 48 (1993) 3160.

[25] S. Catani, Yu.L. Dokshitzer, M.H. Seymour and B.R. Webber, Nucl. Phys. B406 (1993) 187.

[26] G. Ingelman, A. Edin and J. Rathsman, Comp. Phys. Comm. 101 (1997) 108; version used: 6.5.

[27] M. Bengtsson and T. Sjöstrand, Z. Phys. C 37 (1998) 465.

[28] V.N. Gribov and L.N. Lipatov, Sov. J. Nucl. Phys. 15 (1972) 438 and 675;
Yu.L. Dokshitzer, Sov. Phys. JETP 46 (1977) 641;
G. Altarelli and G. Parisi, Nucl. Phys. 126 (1977) 297.

[29] B. Andersson et al., Phys. Rep. 97 (1983) 31.

[30] T. Sjöstrand, Comp. Phys. Comm. 39 (1986) 347; T. Sjöstrand and M. Bengtsson, ibid. 43 (1987) 367.

[31] G. Marchesini et al., Comp. Phys. Comm. 67 (1992) 465; version used: 5.9.

[32] B.R. Webber, Nucl. Phys. B 238 (1984) 492.

[33] L. Lönnblad, Comp. Phys. Comm. 71 (1992) 15; version used: 4.08.

[34] G. Gustafson and U. Petterson, Nucl. Phys. B 306 (1988);
G. Gustafson, Phys. Lett. B 175 (1986) 453;
B. Andersson, G. Gustafson, L. Lönnblad and U. Petterson, Z. Phys. C 43 (1989) 625.

[35] L. Lönnblad, Z. Phys. C 65 (1995) 285.

[36] K. Charchula, G. Schuler and H. Spiesberger, Comp. Phys. Comm. 81 (1994) 381; version used: 6.2.

[37] A. Kwiatkowski, H. Spiesberger and H.-J. Möhring, Comp. Phys. Comm. 69 (1992) 155.

[38] J. Spiekermann, Ph. D. Thesis, University of Dortmund, Dortmund, Germany (1997);
H. Rick, Ph. D. Thesis, University of Dortmund, Dortmund, Germany (1997).

[39] L. Sonnenschein, Diploma-thesis, PITHA 98/4, Aachen, Germany (1998).

[40] R. Engel, Z. Phys. C 66 (1995) 203; R. Engel and J. Ranft, Phys. Rev. D 54 (1996) 4244.

[41] OPAL Collab., G. Abbiendi et al. , CERN-EP/98113, hep-ex/9808027, Geneva, Switzerland, submitted to Eur. Phy. J. C.

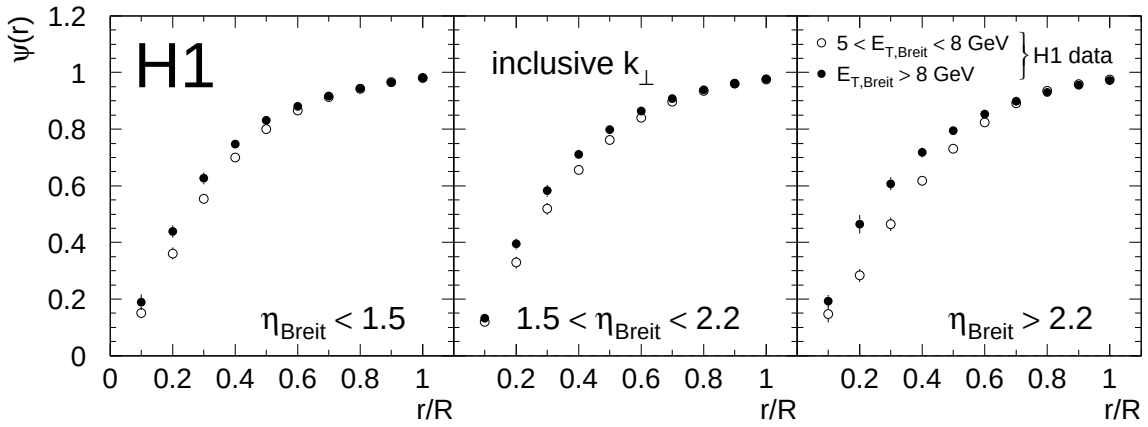

Figure 1: The dependence of the jet shapes on the transverse jet energy in three pseudo-rapidity regions. The jet shapes at higher and at lower transverse jet energies for the inclusive $k_\perp$ algorithm are overlaid. The comparison is shown as a function of the jet pseudo-rapidity in the Breit frame (positive pseudo-rapidities are towards the proton direction).

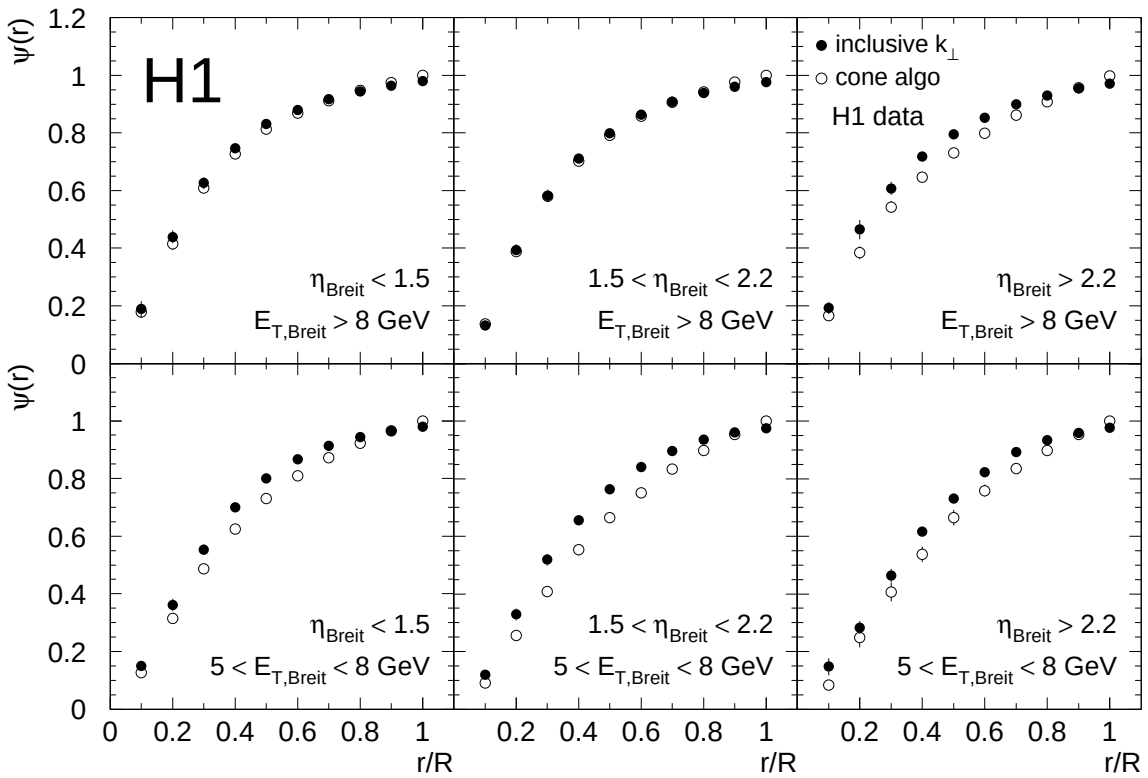

Figure 2: Comparison of the jet shapes for the inclusive $k_\perp$ algorithm and the cone algorithm. The data are shown as a function of the transverse jet energy and the jet pseudo-rapidity in the Breit frame (positive pseudo-rapidities are towards the proton direction).

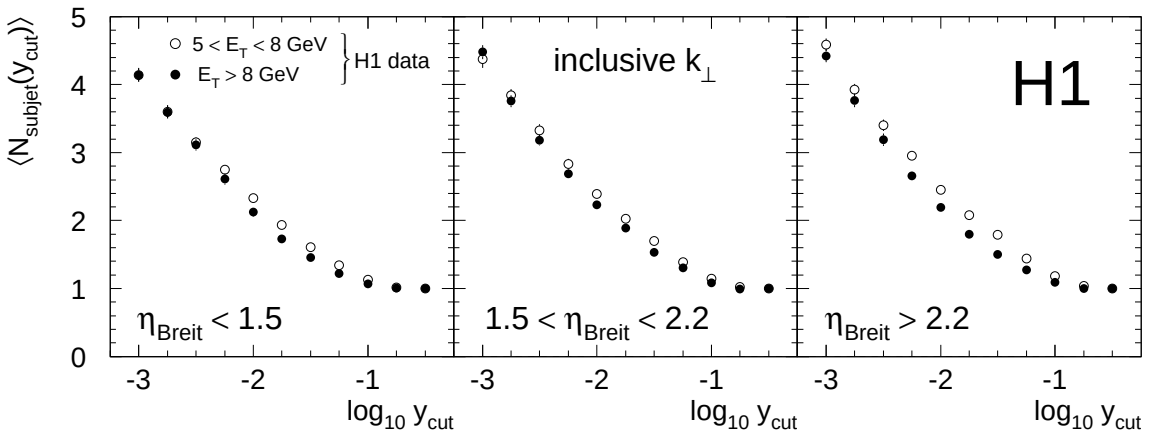

Figure 3: The average number of subjets as a function of the resolution parameter $y_{\rm cut}$ for the inclusive $k_\perp$ algorithm. The data are shown in $\eta_{\rm Breit}$ bins for different $E_{T,\rm Breit}$.

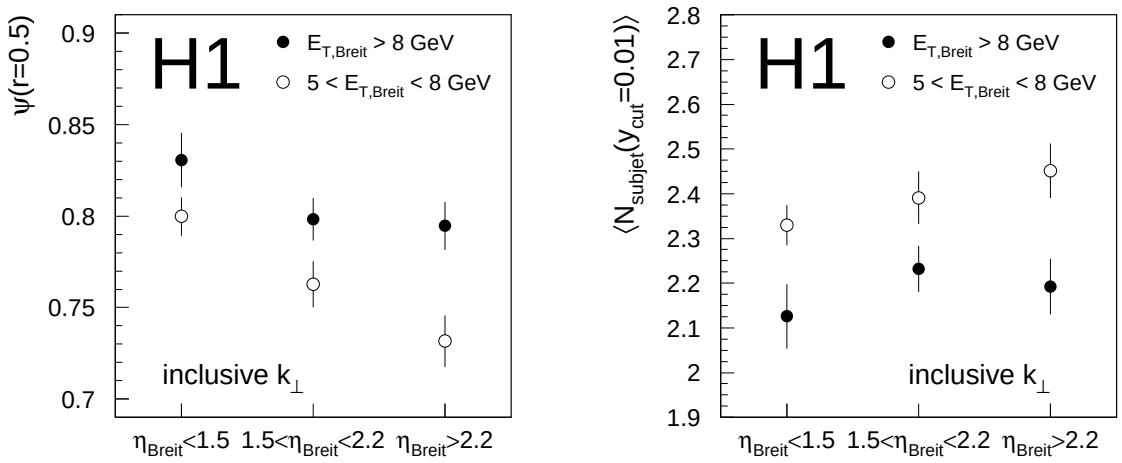

Figure 4: The jet shape $\Psi(r)$ at a fixed subcone radius $r = 0.5$ in three $\eta_{\rm Breit}$ ranges and two $E_{T,\rm Breit}$ bins for the inclusive $k_\perp$ algorithm (left). The average subjet multiplicity at a fixed resolution parameter $y_{\rm cut} = 0.01$ in three $\eta_{\rm Breit}$ ranges and two $E_{T,\rm Breit}$ bins for the inclusive $k_\perp$ algorithm (right). Positive pseudo-rapidities are towards the proton direction.

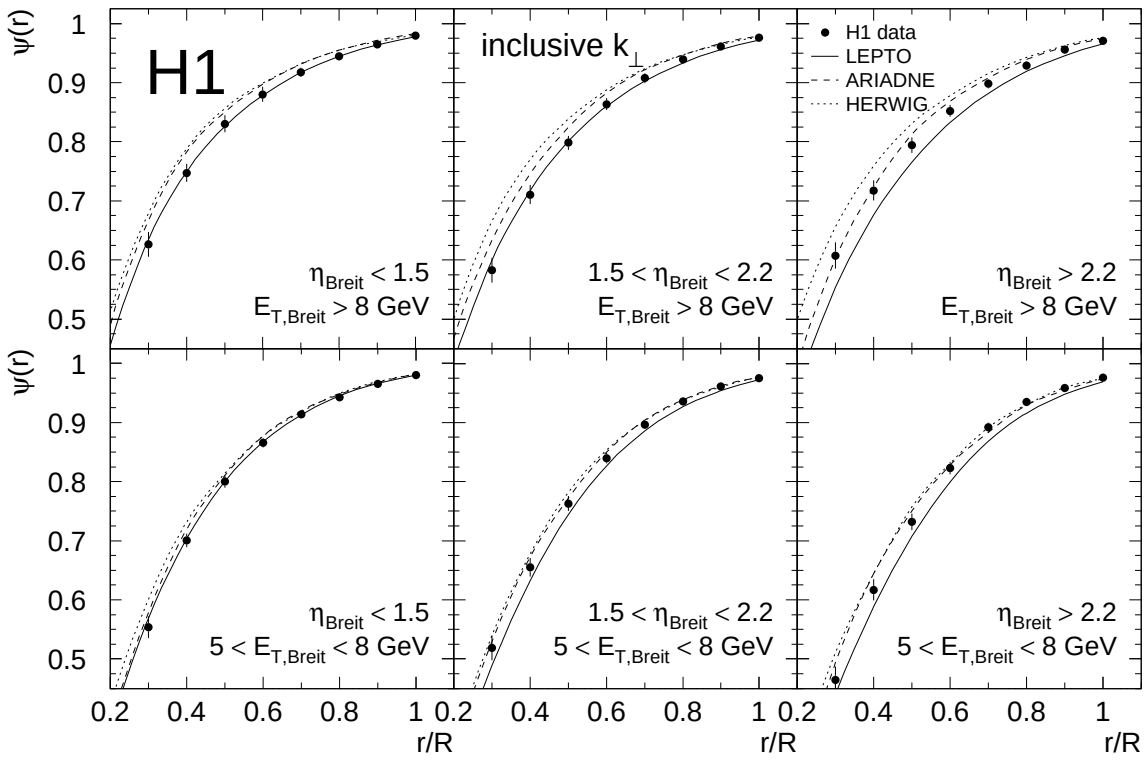

Figure 5: The jet shapes for the inclusive $k_\perp$ algorithm. The data are shown as a function of the transverse jet energy and the jet pseudo-rapidity in the Breit frame (positive pseudo-rapidities are towards the proton direction). The results are compared to predictions of QCD models.

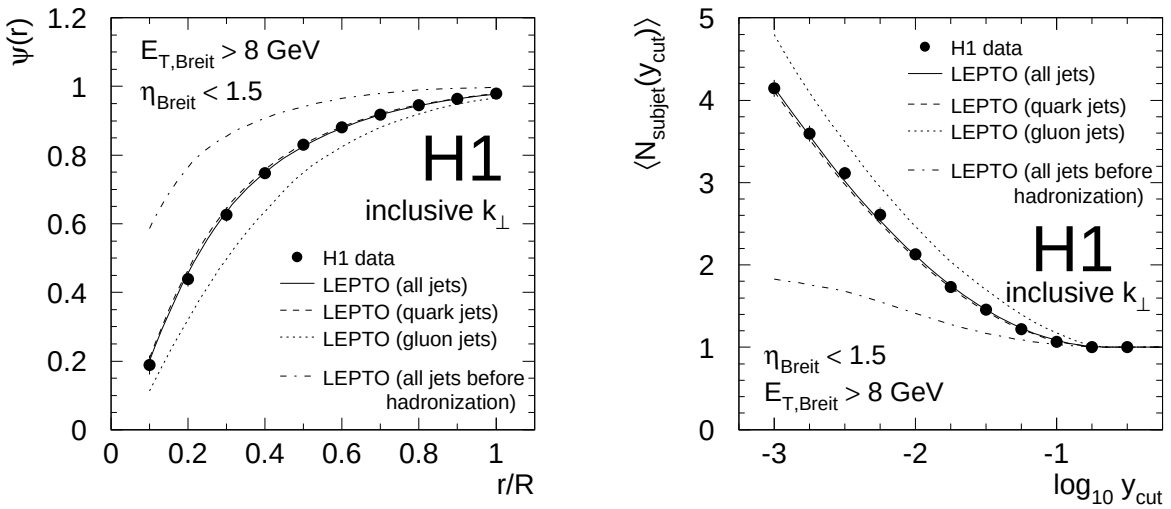

Figure 6: Model predictions of the internal structure of quark and gluon jets for the inclusive $k_\perp$ algorithm by the LEPTO parton shower model. The jet shapes (left) and the subjet multiplicities (right) are shown separately for quark and gluon induced jets with $E_{T,\mathrm{Breit}} > 8\,\mathrm{GeV}$ and $\eta_{\mathrm{Breit}} < 1.5$, together with the sum of both and the comparison to the H1 measurement. The distributions of the observables before hadronization are also shown.